Influence of Bevacizumab on Blood–Brain Barrier Permeability and *O*-(2-^{18}F-Fluoroethyl)-L-Tyrosine Uptake in Rat Gliomas

Carina Stegmayr[1], Dennis Oliveira[1], Nicole Niemietz[1], Antje Willuweit[1], Philipp Lohmann[1], Norbert Galldiks[1,2], N. Jon Shah[1,3,4], Johannes Ermert[1,5], and Karl-Josef Langen[1,5]

[1]Institute of Neuroscience and Medicine (INM-3, INM-4, INM-5, INM-11), Forschungszentrum Jülich, Jülich, Germany; [2]Department of Neurology, University of Cologne, Cologne, Germany; [3]Department of Neurology, RWTH University, Aachen, Germany; [4]Jülich-Aachen Research Alliance (JARA)–Section JARA-Brain, RWTH Aachen University, Aachen, Germany; and [5]Department of Nuclear Medicine, RWTH University Hospital, Aachen, Germany

Restoration of the blood–brain barrier (BBB) after antiangiogenic therapy of gliomas with bevacizumab may result in a decrease in contrast enhancement on MRI despite tumor progression. This so-called pseudoresponse is difficult to differentiate from a true tumor response with conventional MRI. Initial patient studies have indicated that PET using *O*-(2-^{18}F-fluoroethyl)-L-tyrosine (^{18}F-FET) may be helpful for solving this diagnostic problem. This study was performed to investigate the effects of bevacizumab on BBB permeability and ^{18}F-FET uptake in a human xenograft model. **Methods:** Human U87 glioblastoma cells were implanted into the striatum of immunodeficient RNU rats. ^{18}F-FET PET scans and ex vivo autoradiography were performed in animals receiving a single high dose of bevacizumab (45 mg/kg 2 d before PET; $n = 9$) or in animals receiving 2 lower doses (10 mg/kg 9 and 2 d before PET; $n = 10$) to evaluate short-term and long-term effects on the BBB, respectively, and in control animals without bevacizumab treatment ($n = 8$). Time–activity curves, slope, and tumor-to-brain ratios of ^{18}F-FET uptake (18–61 min after injection) were evaluated using a volume-of-interest analysis. After PET scanning, Evans blue dye (EBD) was injected into animals, and cryosections of the brains were evaluated by autoradiography, by histology, and for EBD fluorescence to assess BBB permeability. **Results:** Compared with the control, short-term bevacizumab therapy resulted in a trend toward BBB restoration ($P = 0.055$) and long-term therapy resulted in a significant decrease ($P = 0.004$) in BBB permeability, as assessed by EBD fluorescence. In contrast, no significant differences in tumor-to-brain ratios or slope of ^{18}F-FET uptake were observed in PET and autoradiography ($P > 0.05$). **Conclusion:** ^{8}F-FET uptake in glioblastomas seems to be largely independent of BBB permeability and reflects the viability of tumor tissue during antiangiogenic therapy more reliably than contrast-enhanced MRI.

Key Words: PET; glioblastoma; ^{18}F-FET PET; blood–brain barrier; bevacizumab; Evans blue dye

J Nucl Med 2017; 58:700–705
DOI: 10.2967/jnumed.116.187047

Brain tumor diagnostics using PET with radiolabeled amino acids, such as L-[methyl-^{11}C]methionine (^{11}C-MET), *O*-(2-^{18}F-fluoroethyl)-L-tyrosine (^{18}F-FET), or 3,4-dihydroxy-6-^{18}F-fluoro-L-phenylalanine (^{18}F-FDOPA), are gaining interest and were recently recommended by the Response Assessment in Neuro-Oncology Working Group for every stage of management of patients with brain tumors (*1,2*). Amino acid PET provides important information beyond that provided by standard MRI with respect to delineation of the extent of tumor for biopsy guidance or resection planning, estimation of prognosis, grading, differentiation of treatment-related effects from tumor progression, and treatment monitoring (*3–13*). Compared with ^{11}C-MET, ^{18}F-FET and ^{18}F-FDOPA have logistic advantages because of the longer half-life of ^{18}F (110 vs. 20 min) (*14–18*).

The humanized monoclonal antibody bevacizumab (Avastin; Genentech/Roche) inhibits the biologic activity of vascular endothelial growth factor. From 2007 to 2014, bevacizumab was intensively evaluated in phase 2 and 3 trials, particularly in the early phase of the course of malignant gliomas—that is, in newly diagnosed glioblastomas or at first recurrence or progression (*19*). However, at this stage of disease, the use of bevacizumab has not improved overall survival (*20*). Currently, bevacizumab is frequently used in many neurooncologic centers at a late stage of disease, particularly when standard treatment options—such as surgery, radiation, and alkylating chemotherapy—are no longer helpful or possible or when a reduction in the corticosteroid dosage for symptomatic therapy is considered. Bevacizumab is usually administered intravenously (10 mg/kg every 2 wk) as a single agent or as a combined therapy. Treatment influences brain tumor vasculature and leads to restoration of the blood–brain barrier (BBB), resulting in decreased contrast enhancement on MRI and reduced peritumoral edema. An important problem in the follow-up of malignant glioma, however, is a decrease in contrast enhancement on MRI after antiangiogenic therapy with bevacizumab; this feature does not reflect a true antitumoral effect and is called a pseudoresponse (*21*). This decrease in contrast enhancement caused by restoration of the BBB can be mistaken for a treatment response, as MRI contrast enhancement primarily reflects impairment of the BBB (*22*).

The Response Assessment in Neuro-Oncology Working Group suggested new recommendations for evaluating the

Received Nov. 11, 2016; revision accepted Dec. 26, 2016.
For correspondence or reprints contact: Karl-Josef Langen, Institute of Neuroscience and Medicine, Research Center Jülich, D-52425 Jülich, Germany.
E-mail: k.j.langen@fz-juelich.de
Published online Feb. 2, 2017.

response to antiangiogenic drugs, including fluid-attenuated inversion recovery or T2 signal alterations, as criteria for determining tumor response or progression (*23*). However, these new criteria do not provide quantitative values, and various pathologies can result in hyperintense fluid-attenuated inversion recovery or T2 signal alterations, which are difficult to distinguish from a nonenhancing tumor (*21*). Consequently, alternative diagnostic methods are needed to assess the effects of bevacizumab treatment (*24*).

Dynamic ^{18}F-FET PET has been shown to be superior to other imaging methods for differentiating progression from nonneoplastic changes (*7,10,25*). Initial pilot studies with this technique for bevacizumab treatment monitoring in patients with malignant gliomas demonstrated that PET using ^{18}F-FET detected treatment failure earlier than MRI—on the basis of the criteria of the Response Assessment in Neuro-Oncology Working Group—and predicted favorable outcomes of responders (*26–28*). However, data on the influence of bevacizumab-related alterations of the BBB on ^{18}F-FET uptake are limited, and further evaluation is needed.

In this preclinical study, the influence of antiangiogenic treatment with bevacizumab on BBB integrity, ^{18}F-FET uptake, and the slope of the late phase of the time–activity curve was tested in a U87 human glioblastoma xenograft model. This tumor model was chosen because it is largely resistant to bevacizumab on the one hand but shows a significant decrease in contrast enhancement on MRI after bevacizumab treatment on the other hand (*29,30*). Therefore, it appears to be well suited for simulating the phenomenon of the pseudoresponse and for testing the role of ^{18}F-FET PET in this setting.

MATERIALS AND METHODS

Animals

Twenty-seven male immunodeficient RNU rats (Charles River Laboratories) were included in this study. All animals were handled in accordance with the Animal Research Committee of the Research Center Jülich GmbH, the German Animal Welfare Act, and the European Community Council directives regarding the protection of animals used for experimental and scientific purposes (2010/63/EU). All rats weighed 250–310 g and were kept under standard housing conditions with free access to food and water. Human U87 glioma cells were implanted into the striatum of the animals, and the presence of a brain tumor was verified by histologic staining with 4′,6-diamidino-2-phenylindole (DAPI) after completion of the studies.

Animals were divided into a control group ($n = 8$), a group receiving short-term bevacizumab treatment ($n = 9$), and a group receiving long-term bevacizumab treatment ($n = 10$). All animals were sacrificed after ^{18}F-FET PET, and cryosections of the brains were analyzed by autoradiography (AR), by histology, and for Evans blue dye (EBD) fluorescence to assess BBB permeability.

Tumor Inoculation and Bevacizumab Treatment

U87 cells (HTB-14; American Type Culture Collection) were cultured in Eagle minimum essential medium supplemented with 10% fetal calf serum, penicillin/streptomycin, glutamate, and 1% nonessential amino acids. At a confluence of approximately 95%, cells were prepared for inoculation. Cells were washed twice with phosphate-buffered saline and detached by incubation with trypsin/ethylenediaminetetraacetic acid for approximately 5 min. Cells were resolved in growth medium to a concentration of 500,000 per 5-μL implantation volume. Cells were stereotactically implanted into the right basal ganglia under anesthesia as described previously (*31*). PET scans, EBD staining (2% EBD [500 μL/kg] in NaCl, administered intravenously 30 min before sacrifice), and histologic evaluations were performed on day 13 or 14 after tumor implantation.

Rats receiving long-term bevacizumab treatment ($n = 10$) received 2 injections of bevacizumab (10 mg/kg intravenously) 9 and 2 d before ^{18}F-FET PET. Rats receiving short-term bevacizumab treatment ($n = 9$) received 1 injection (45 mg/kg intravenously) 2 d before ^{18}F-FET PET. The control group ($n = 8$) received no treatment. For technical reasons, only 6 rats from the control group were evaluated for EBD extravasation and by AR.

Imaging Methods

After isoflurane anesthetization, a venous catheter was inserted into 1 tail vein. The rats were positioned in the field of view of a small-animal scanner (INVEON; Siemens-CTI) (*32*). Body temperature was maintained at 37.8°C ± 0.3°C (mean ± SD) with an infrared lamp. Breathing rate was regulated at 48–55 breaths/min with a pressure-sensitive pad positioned under the rats. ^{18}F-FET with a specific radioactivity of greater than 200 GBq/μmol was synthesized in-house as described elsewhere (*33*). After a transmission scan (10–20 min), dynamic data acquisition was performed in the 3-dimensional list mode for 61 min starting with an injection of 40 ± 3 MBq of ^{18}F-FET in saline into the tail vein (bolus injection of 0.5 mL in 1 min). Emission data were framed into a dynamic sequence of 6 × 10 s, 5 × 60 s, 5 × 3 min, and 10 × 4 min frames. Filtered backprojection (ramp filter; cutoff, 0.5) was applied to reconstruct 159 slices with an image voxel size of 0.7764 × 0.7764 × 0.796 mm (matrix size, 128 × 128 × 159). Images were corrected for random coincidences, scatter radiation, and attenuation. Because an INVEON software update during the course of the experiments affected data reconstruction, a calibration factor of 1.20 was applied to a portion of the data to guarantee comparability. After the PET scan and EBD injection, rats were sacrificed.

Brains were removed, quickly frozen in liquid isopentane (−50°C), and cut into 20-μm-thick slices with a cryostat. The presence of a brain tumor was verified by fluorescence staining with DAPI. EBD extravasation was evaluated quantitatively on the basis of fluorescence intensity per animal by defining regions of interest in a single brain slice in the area of the tumor with an Aida Image Analyzer (AIDA version 4.50; Raytest). Regions of interest were placed in healthy contralateral tissue and in the tumor after consideration of histologic staining. EBD extravasation in the tumor area is reported as tumor-to-brain ratios (TBRs).

For AR, an imaging plate (Fuji Imaging Plate; Raytest) was exposed overnight to every tenth slice and freshly prepared 20-μm ^{18}F standards for a calibration curve; samples were scanned (Fuji BAS Reader 5000; Raytest) and evaluated for ^{18}F-FET uptake in a pixel size of 200 μm (AIDA version 4.50).

Anti–von Willebrand factor antibody (ab6994; Abcam) staining was performed using a standard protocol for diaminobenzidine staining to visualize blood vessels. Cell nuclei were counterstained with hematoxylin.

Data Analysis

Analysis of PET data was performed with Pmod version 3.4 (PMOD Technologies Ltd.). ^{18}F-FET uptake in the tissue was expressed as the SUV by dividing the radioactivity (kBq/mL) in the tissue by the radioactivity injected per gram of body weight. Summed PET images (18–61 min after injection) were used for volume-of-interest (VOI) analysis as described previously (*34*). The tumor VOI on ^{18}F-FET PET scans was determined by a 3-dimensional autocontouring process with a cutoff of greater than or equal to 1.7 for the TBR of

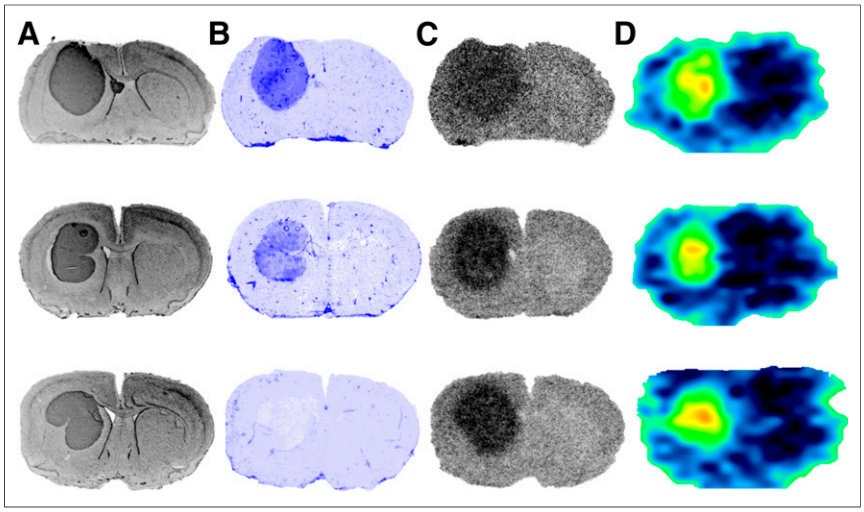

FIGURE 1. Overviews of different imaging methods. (A) DAPI nuclear stains show tumor dimensions. (B) EBD fluorescence images show BBB impairment. (C) Ex vivo autoradiographs show ^{18}F-FET uptake 65 min after injection. (D) Summed PET images (18–61 min after injection) show ^{18}F-FET accumulation. (Top) Representative brain from baseline group. (Middle) Representative brain from group receiving short-term bevacizumab treatment. (Bottom) Representative brain from group receiving long-term bevacizumab treatment.

^{18}F-FET uptake; this cutoff proved to be reliable for indicating the actual tumor size (*34*). ^{18}F-FET uptake in the unaffected brain tissue was determined from a larger VOI placed in an area of normal brain tissue including white and gray matter (250 voxels; 120 mm^3) in the contralateral hemisphere. The mean TBR (TBR_{mean}) was calculated by dividing the mean VOI (Bq/mL) of the tumor by the mean VOI of normal brain tissue; the maximum TBR (TBR_{max}) was calculated by dividing the maximum VOI (5 hottest voxels) of the tumor by the mean VOI of normal brain tissue. A linear regression line was fitted to the late phase of time–activity curves (18–61 min after injection) to determine the slope.

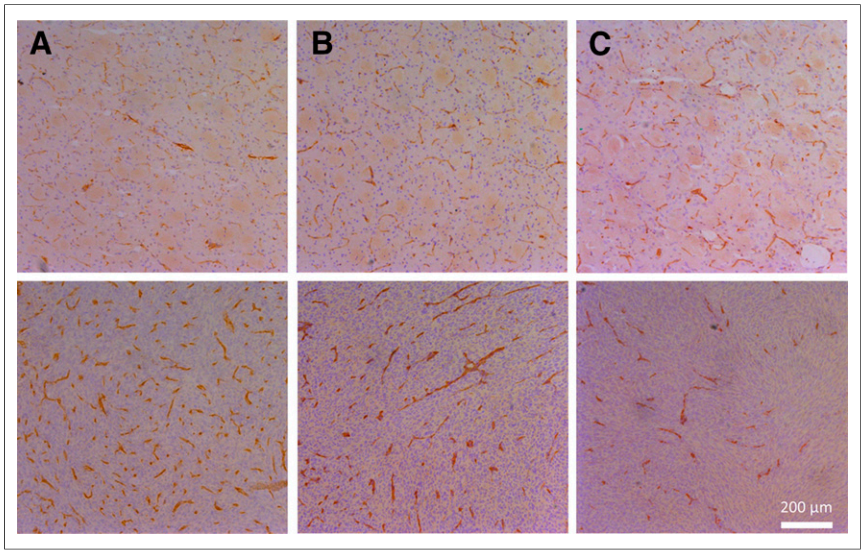

FIGURE 2. Blood vessel staining. (Top) Results of staining of blood vessel endothelia (brown) in contralateral tissue were similar for control group (A), group receiving short-term bevacizumab treatment (B), and group receiving long-term bevacizumab treatment (C). (Bottom) Tumor vessels in control group (A) and group receiving short-term bevacizumab treatment (B) were large and dense, whereas fewer and smaller vessels were detected in group receiving long-term bevacizumab treatment (C).

Statistics

Descriptive statistics are provided as mean and SD. One-way ANOVAs with all pairwise multiple-comparison procedures (Holm–Sidak method) were performed for PET data, EBD evaluations, and AR to detect differences among the treatments without correction for multiple testing. *P* values of less than or equal to 0.05 were considered significant. Statistical analysis was performed using SigmaPlot for Windows version 12.5 (Systat Software, Inc.).

RESULTS

Consecutive representative overviews of histologic DAPI staining, EBD fluorescence, AR, and corresponding ^{18}F-FET uptake from PET scans of a control brain, a brain receiving short-term treatment with bevacizumab, and a brain receiving long-term treatment with bevacizumab are shown in Figure 1. In the control group, intense EBD fluorescence indicated BBB impairment in the area of the tumor, whereas fluorescence was less intense in the group receiving short-term treatment and no longer visible in the group receiving long-term treatment. ^{18}F-FET uptake in AR was restricted to the tumor areas, and summed images (18–61 min after injection) seemed to be unaffected by bevacizumab treatment (Figs. 1C and 1D) despite a reduction in BBB permeability (Fig. 1B).

Vascular staining revealed normal blood vessels in contralateral tissue in all 3 groups, whereas vessels in untreated tumors and tumors receiving short-term treatment were dense and larger than those in normal tissue. In tumors receiving long-term treatment, the number of vessels was considerably diminished, and the vessels were smaller (Fig. 2).

Using ANOVAs, we confirmed the stability of ^{18}F-FET uptake shown by the TBR_{mean} from AR (control, 2.04 ± 0.30; short-term treatment, 1.89 ± 0.08; long-term treatment, 1.89 ± 0.24; $P = 0.419$) and PET, as bevacizumab treatment did not significantly influence the factors TBR_{mean}, TBR_{max}, and slope. The area under the curve for the group receiving long-term treatment was significantly smaller than that for the control group ($P = 0.002$) (Table 1). The tumor volume, as defined by the VOI, was smallest in the group receiving long-term treatment but, because of the great variance in tumor sizes, the difference was not significant.

These results are underlined by the similarity of time–activity curves from 20 min after injection in all 3 groups, as shown in Figure 3. Bevacizumab treatment also did not influence ^{18}F-FET uptake in normal brain tissue (Fig. 3).

Although the ^{18}F-FET TBR_{mean} and TBR_{max} remained unchanged with bevacizumab treatment, BBB permeability—as

TABLE 1
PET-Derived Values

Parameter	Group*			*P*	
	Baseline (b)†	Short-term treatment (st)‡	Long-term treatment (lt)§	ANOVA	Holm–Sidak method‖
TBR_{mean} 18–61 min after injection	1.90 ± 0.10	1.89 ± 0.10	1.85 ± 0.06	NS (0.494)	
TBR_{max} 18–61 min after injection	2.21 ± 0.26	2.17 ± 0.23	2.09 ± 0.15	NS (0.541)	b vs. lt: 0.002
AUC for tumor	94.97 ± 6.63	89.09 ± 6.50	83.28 ± 5.42	0.002	b vs. st: 0.061
Slope for tumor (SUV/h)	0.12 ± 0.07	0.09 ± 0.10	0.16 ± 0.10	NS (0.278)	st vs. lt: 0.100
Tumor volume (mm^3)	44.14 ± 17.71	69.09 ± 87.61	39.38 ± 17.11	NS (0.305)	

*Reported as mean ± SD.
†$n = 8$.
‡$n = 9$.
§$n = 10$.
‖*P* values from post hoc test (Holm–Sidak method) are reported when differences were significant.
NS = not significant; AUC = area under curve; slope = slope of time–activity curve for ^{18}F-FET uptake 18–61 min after injection.

measured by EBD extravasation—decreased, depending on the duration of the treatment rather than the dose. A high dose (45 mg/kg) 48 h before the final scan (short-term treatment) resulted in a trend toward BBB restoration (control, 4.00 ± 2.01; short-term treatment, 2.43 ± 1.04), but only long-term treatment with 2 doses of bevacizumab (10 mg/kg) 2 and 9 d before the final scan had a significant impact on BBB permeability (control, 4.00 ± 2.01; long-term treatment, 1.73 ± 0.45; $P = 0.014$) (Fig. 4).

DISCUSSION

PET using ^{18}F-FET is increasingly being accepted as a complementary tool for brain tumor diagnostics and therapy monitoring. The influence of BBB disruption on ^{18}F-FET uptake, however, is a matter of continued discussion because there is a significant correlation between contrast enhancement on MRI and ^{18}F-FET or ^{11}C-MET accumulation in brain tumors with different grades of malignancy (*35,36*). This correlation, however, is probably attributable to the fact that the degree of contrast enhancement on MRI on the one hand and ^{18}F-FET or ^{11}C-MET uptake on the other hand is more pronounced in malignant tumors than in low-grade tumors and leads to the assumption of a causal relationship between the parameters (*37*). Experimental studies have demonstrated that the uptake of ^{18}F-FET by brain tumors is dominated by increased transport via transport system L for large neutral amino acids—namely, the subtypes LAT1 and LAT2—which are expressed at the intact BBB (*38*).

Therefore, a disruption of the BBB is not a prerequisite for intratumoral accumulation, and increased ^{18}F-FET uptake has been reported in many low-grade gliomas without BBB leakage (*8,9,39,40*). As opposed to these observations, we hypothesized that if ^{18}F-FET uptake were influenced to a major extent by passive tracer influx across the disrupted BBB, then a restoration of the BBB after bevacizumab treatment should lead to a reduction in tracer uptake similar to the reduction in EBD extravasation.

The results of the present study clearly refute this hypothesis. Although the BBB permeability of U87 tumors—as demonstrated by EBD extravasation—was clearly reduced after long-term bevacizumab therapy, there was no significant effect on the TBR_{mean} and TBR_{max} of ^{18}F-FET uptake in the U87 tumor model. Tumor size seemed to be smaller in the group receiving long-term treatment than in the control group or the group receiving short-term treatment, but the differences were not significant, consis-

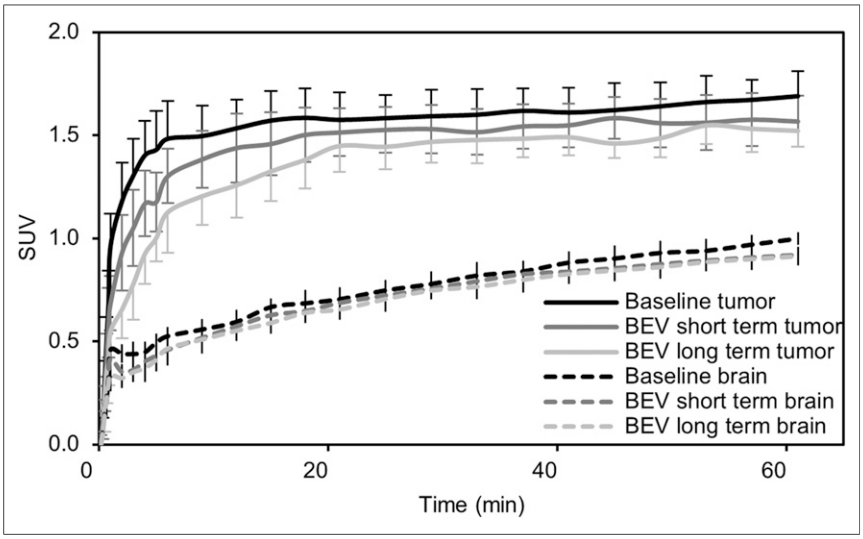

FIGURE 3. Time–activity curves. Graph shows averaged time–activity curves and SDs for ^{18}F-FET uptake (SUV) in all 3 treatment groups. Highest SDs for brain curves were superposed on lower SDs for every time point. Bevacizumab (BEV) treatment reduced tracer uptake in early uptake phase (up to 20 min after injection), but there were no significant differences among treatment groups in later phase.

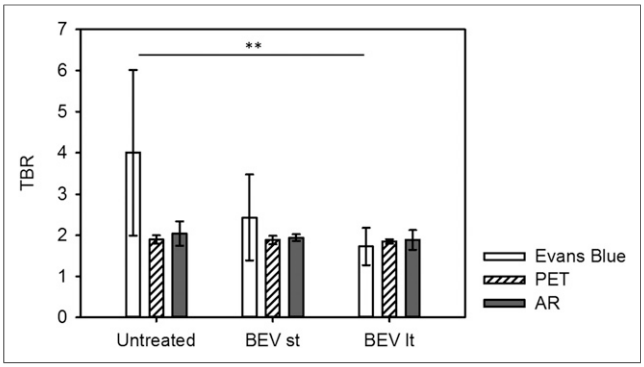

FIGURE 4. Influence of BBB restoration by bevacizumab (BEV) on ^{18}F-FET TBR. Bars show trend toward decrease (P = 0.055) in EBD TBR after short-term treatment (st) with BEV and significant decrease (P = 0.004) after long-term treatment (lt), whereas ^{18}F-FET TBR in PET and AR were constant. **P = 0.004.

tent with the observation of limited reduction in tumor progression in other studies (*29*,*30*).

The results of the present study are in line with those of a previous study using the amino acid tracer ^{3}H-MET and the artificial amino acid *trans*-1-amino-3-fluoro-1-^{14}C-cyclobutanecarboxylic acid in the U87 tumor model (*30*). Therefore, the present study confirms the previous experimental and clinical finding that PET using ^{18}F-FET and other amino acid tracers is able to disclose the phenomenon of pseudoprogression, which is a frequent diagnostic problem in conventional MRI during antiangiogenic therapy. This method may allow the earlier detection of treatment failure so that unnecessary adverse effects can be avoided.

Another important aspect of the present study was the influence of bevacizumab treatment on the time–activity curve of ^{18}F-FET uptake. Several studies have demonstrated that evaluation of the time–activity curve of ^{18}F-FET uptake in tumors may be helpful for estimating tumor aggressiveness (*9*–*13*). High-grade gliomas are characterized by an early peak in the time–activity curve, at about 10–15 min after tracer injection, followed by a decrease in ^{18}F-FET uptake; the time–activity curve of low-grade gliomas (World Health Organization grade II) slightly and steadily increases (*10*,*12*). It has been suggested that the decrease in ^{18}F-FET uptake in high-grade gliomas is influenced by facilitated backdiffusion of unbound tracer due to BBB leakage (*12*). The results of the present study indicated that restoration of the BBB by bevacizumab treatment did not influence the slope of the time–activity curve of ^{18}F-FET uptake in the late phase of tracer uptake. However, bevacizumab treatment did have an influence on the early accumulation phase, which was delayed—especially in animals receiving long-term treatment—and which had a significant impact on the area under the curve (Table 1). This observation may reflect reduced vascularization (Fig. 2), as the signal from ^{18}F-FET radioactivity in the blood pool was high during the first 15 min after injection (*16*). However, this possibility can be analyzed only by pharmacokinetic modeling, which was not available in our experimental setup.

Several experimental studies have already examined the usefulness of different PET tracers for monitoring antiangiogenic therapy (*30*). Beyond radiolabeled amino acids, the proliferation tracer 3′-deoxy-3′-^{18}F-fluorothymidine (^{18}F-FLT) has been investigated in 2 clinical trials (*41*,*42*). A reduction in ^{18}F-FLT uptake after bevacizumab treatment had a high predictive value for the survival time of patients, but a limitation of this tracer is that BBB breakdown is a prerequisite for ^{18}F-FLT uptake—and even high-grade gliomas with a high proliferation index may be ^{18}F-FLT–negative if they lack contrast enhancement on MRI (*24*).

Finally, animal models may not correctly reflect the human situation. Although the human xenograft model may be more appropriate than rat glioma models, the biologic properties and growth patterns of implanted tumors differ from those of human tumors. For example, the time–activity curve of ^{18}F-FET uptake in the U87 tumor model exhibited a plateau phase beyond 20 min after injection, whereas human glioblastomas usually show a decreasing time–activity curve in the late phase. Furthermore, for the specific issue in the present study, a cell line that was largely resistant to bevacizumab was selected. Therefore, the data should be considered with caution. Nevertheless, the experiments provide convincing evidence for the relationship of ^{18}F-FET uptake and BBB permeability and confirm the observations in humans in previous studies (*26*,*27*).

CONCLUSION

The results of this experimental study suggested that monitoring of antiangiogenic therapy in glioblastomas with ^{18}F-FET PET seems to be largely independent of BBB permeability and could solve the problem of the pseudoresponse in contrast-enhanced MRI. This method may allow the earlier detection of treatment failure so that overtreatment and unnecessary adverse effects can be avoided.

DISCLOSURE

No potential conflict of interest relevant to this article was reported.

ACKNOWLEDGMENTS

We thank Michaela Bohlen, Melanie Heymann, and Larissa Grochowski for animal husbandry and Erika Wabbals, Silke Grafmüller, and Sascha Rehbein for technical assistance in the radiosynthesis of ^{18}F-FET.

REFERENCES

1. Langen KJ, Watts C. Neuro-oncology: amino acid PET for brain tumours—ready for the clinic? *Nat Rev Neurol.* 2016;12:375–376.
2. Albert NL, Weller M, Suchorska B, et al. Response Assessment in Neuro-Oncology Working Group and European Association for Neuro-Oncology recommendations for the clinical use of PET imaging in gliomas. *Neuro Oncol.* 2016;18:1199–1208.
3. Galldiks N, Langen K, Holy R, et al. Assessment of treatment response in patients with glioblastoma using [^{18}F]fluoroethyl-L-tyrosine PET in comparison to MRI. *J Nucl Med.* 2012;53:1048–1057.
4. Pauleit D, Floeth F, Hamacher K, et al. *O*-(2-[^{18}F]fluoroethyl)-L-tyrosine PET combined with MRI improves the diagnostic assessment of cerebral gliomas. *Brain.* 2005;128:678–687.
5. Pauleit D, Stoffels G, Bachofner A, et al. Comparison of ^{18}F-FET and ^{18}F-FDG PET in brain tumors. *Nucl Med Biol.* 2009;36:779–787.
6. Pichler R, Dunzinger A, Wurm G, et al. Is there a place for FET PET in the initial evaluation of brain lesions with unknown significance? *Eur J Nucl Med Mol Imaging.* 2010;37:1521–1528.
7. Pöpperl G, Gotz C, Rachinger W, Gildehaus FJ, Tonn JC, Tatsch K. Value of *O*-(2-[^{18}F]fluoroethyl)-L-tyrosine PET for the diagnosis of recurrent glioma. *Eur J Nucl Med Mol Imaging.* 2004;31:1464–1470.
8. Floeth FW, Pauleit D, Sabel M, et al. Prognostic value of *O*-(2-^{18}F-fluoroethyl)-L-tyrosine PET and MRI in low-grade glioma. *J Nucl Med.* 2007;48:519–527.
9. Jansen NL, Suchorska B, Wenter V, et al. Prognostic significance of dynamic ^{18}F-FET PET in newly diagnosed astrocytic high-grade glioma. *J Nucl Med.* 2015;56:9–15.
10. Pöpperl G, Kreth FW, Herms J, et al. Analysis of ^{18}F-FET PET for grading of recurrent gliomas: is evaluation of uptake kinetics superior to standard methods? *J Nucl Med.* 2006;47:393–403.
11. Pöpperl G, Kreth FW, Mehrkens JH, et al. FET PET for the evaluation of untreated gliomas: correlation of FET uptake and uptake kinetics with tumour grading. *Eur J Nucl Med Mol Imaging.* 2007;34:1933–1942.

12. Weckesser M, Langen KJ, Rickert CH, et al. *O*-(2-[^{18}F]fluorethyl)-L-tyrosine PET in the clinical evaluation of primary brain tumours. *Eur J Nucl Med Mol Imaging.* 2005;32:422–429.
13. Calcagni ML, Galli G, Giordano A, et al. Dynamic *O*-(2-[^{18}F]fluoroethyl)-L-tyrosine (F-18 FET) PET for glioma grading: assessment of individual probability of malignancy. *Clin Nucl Med.* 2011;36:841–847.
14. Galldiks N, Langen KJ. Applications of PET imaging of neurological tumors with radiolabeled amino acids. *Q J Nucl Med Mol Imaging.* 2015;59:70–82.
15. Herholz K, Langen KJ, Schiepers C, Mountz JM. Brain tumors. *Semin Nucl Med.* 2012;42:356–370.
16. Langen KJ, Hamacher K, Weckesser M, et al. *O*-(2-[^{18}F]fluoroethyl)-L-tyrosine: uptake mechanisms and clinical applications. *Nucl Med Biol.* 2006;33:287–294.
17. Wester HJ, Herz M, Weber W, et al. Synthesis and radiopharmacology of *O*-(2-[^{18}F]fluoroethyl)-L-tyrosine for tumor imaging. *J Nucl Med.* 1999;40:205–212.
18. Galldiks N, Stoffels G, Filss C, et al. The use of dynamic *O*-(2-^{18}F-fluoroethyl)-L-tyrosine PET in the diagnosis of patients with progressive and recurrent glioma. *Neuro Oncol.* 2015;17:1293–1300.
19. Taal W, Oosterkamp HM, Walenkamp AM, et al. Single-agent bevacizumab or lomustine versus a combination of bevacizumab plus lomustine in patients with recurrent glioblastoma (BELOB trial): a randomised controlled phase 2 trial. *Lancet Oncol.* 2014;15:943–953.
20. Chinot OL, Wick W, Mason W, et al. Bevacizumab plus radiotherapy–temozolomide for newly diagnosed glioblastoma. *N Engl J Med.* 2014;370:709–722.
21. Ahluwalia MS, Wen PY. Antiangiogenic therapy for patients with glioblastoma: current challenges in imaging and future directions. *Expert Rev Anticancer Ther.* 2011;11:653–656.
22. Brandsma D, van den Bent MJ. Pseudoprogression and pseudoresponse in the treatment of gliomas. *Curr Opin Neurol.* 2009;22:633–638.
23. Wen PY, Macdonald DR, Reardon DA, et al. Updated response assessment criteria for high-grade gliomas: Response Assessment in Neuro-Oncology Working Group. *J Clin Oncol.* 2010;28:1963–1972.
24. Hutterer M, Hattingen E, Palm C, Proescholdt MA, Hau P. Current standards and new concepts in MRI and PET response assessment of antiangiogenic therapies in high-grade glioma patients. *Neuro Oncol.* 2015;17:784–800.
25. Galldiks N, Stoffels G, Filss CP, et al. Role of *O*-(2-^{18}F-fluoroethyl)-L-tyrosine PET for differentiation of local recurrent brain metastasis from radiation necrosis. *J Nucl Med.* 2012;53:1367–1374.
26. Galldiks N, Rapp M, Stoffels G, et al. Response assessment of bevacizumab in patients with recurrent malignant glioma using [^{18}F]fluoroethyl-L-tyrosine PET in comparison to MRI. *Eur J Nucl Med Mol Imaging.* 2013;40:22–33.
27. Hutterer M, Nowosielski M, Putzer D, et al. *O*-(2-^{18}F-fluoroethyl)-L-tyrosine PET predicts failure of antiangiogenic treatment in patients with recurrent high-grade glioma. *J Nucl Med.* 2011;52:856–864.
28. Galldiks N, Filss CP, Goldbrunner R, Langen KJ. Discrepant MR and [^{18}F] fluoroethyl-L-tyrosine PET imaging findings in a patient with bevacizumab failure. *Case Rep Oncol.* 2012;5:490–494.
29. Mesti T, Savarin P, Triba MN, et al. Metabolic impact of anti-angiogenic agents on U87 glioma cells. *PLoS One.* 2014;9:e99198.
30. Ono T, Sasajima T, Doi Y, et al. Amino acid PET tracers are reliable markers of treatment responses to single-agent or combination therapies including temozolomide, interferon-beta, and/or bevacizumab for glioblastoma. *Nucl Med Biol.* 2015;42:598–607.
31. Langen KJ, Jarosch M, Muhlensiepen H, et al. Comparison of fluorotyrosines and methionine uptake in F98 rat gliomas. *Nucl Med Biol.* 2003;30:501–508.
32. Bao Q, Newport D, Chen M, Stout DB, Chatziioannou AF. Performance evaluation of the Inveon dedicated PET preclinical tomograph based on the NEMA NU-4 standards. *J Nucl Med.* 2009;50:401–408.
33. Hamacher K, Coenen HH. Efficient routine production of the ^{18}F-labelled amino acid *O*-2-^{18}F-fluoroethyl-L-tyrosine. *Appl Radiat Isot.* 2002;57:853–856.
34. Stegmayr C, Schoneck M, Oliveira D, et al. Reproducibility of *O*-(2-^{18}F-fluoroethyl)-L-tyrosine uptake kinetics in brain tumors and influence of corticoid therapy: an experimental study in rat gliomas. *Eur J Nucl Med Mol Imaging.* 2016;43:1115–1123.
35. Hutterer M, Nowosielski M, Putzer D, et al. [F-18]-fluoro-ethyl-L-tyrosine PET: a valuable diagnostic tool in neuro-oncology, but not all that glitters is glioma. *Neuro Oncol.* 2013;15:341–351.
36. Roelcke U, Radu E, Ametamey S, Pellikka R, Steinbrich W, Leenders KL. Association of rubidium and C-methionine uptake in brain tumors measured by positron emission tomography. *J Neurooncol.* 1996;27:163–171.
37. Langen KJ, Galldiks N. Reply to "[^{18}F]-fluoro-ethyl-L-tyrosine PET: a valuable diagnostic tool in neuro-oncology, but not all that glitters is glioma" by Hutterer et al. [letter]. *Neuro Oncol.* 2013;15:816–817.
38. Habermeier A, Graf J, Sandhöfer BF, Boissel JP, Roesch F, Closs EI. System L amino acid transporter LAT1 accumulates *O*-(2-fluoroethyl)-L-tyrosine (FET). *Amino Acids.* 2015;47:335–344.
39. Bette S, Gempt J, Delbridge C, et al. Prognostic value of *O*-(2-[^{18}F]-fluoroethyl)-L-tyrosine-positron emission tomography imaging for histopathologic characteristics and progression-free survival in patients with low-grade glioma. *World Neurosurg.* 2016;89:230–239.
40. Rapp M, Heinzel A, Galldiks N, et al. Diagnostic performance of ^{18}F-FET PET in newly diagnosed cerebral lesions suggestive of glioma. *J Nucl Med.* 2013;54: 229–235.
41. Chen W, Delaloye S, Silverman DH, et al. Predicting treatment response of malignant gliomas to bevacizumab and irinotecan by imaging proliferation with [^{18}F]fluorothymidine positron emission tomography: a pilot study. *J Clin Oncol.* 2007;25:4714–4721.
42. Schwarzenberg J, Czernin J, Cloughesy TF, et al. 3′-deoxy-3′-^{18}F-fluorothymidine PET and MRI for early survival predictions in patients with recurrent malignant glioma treated with bevacizumab. *J Nucl Med.* 2012;53:29–36.